THESIS

EVALUATING POST-FIRE GEOMORPHIC CHANGE ON PAIRED MULCHED AND UNMULCHED CATCHMENTS USING REPEAT DRONE SURVEYS

Submitted by

Lindsey Hayter

Department of Civil & Environmental Engineering

In partial fulfillment of the requirements

For the Degree of Master of Science

Colorado State University

Fort Collins, Colorado

Summer 2023

Master's Committee:

Advisor: Peter Nelson

Stephanie Kampf

Ryan Morrison

ABSTRACT

EVALUATING POST-FIRE GEOMORPHIC CHANGE ON PAIRED MULCHED AND UNMULCHED CATCHMETNS USING REPEAT DRONE SURVEYS

Sediment redistribution after wildfire can dramatically alter a catchment and pose risks to local infrastructure and water quality. Mulch application is increasingly being used to mitigate post-fire hillslope runoff and erosion, although relatively little is known about its effects at the catchment scale. In this study we used repeat drone surveys to measure erosion and deposition across 6 small (0.5-1.5 km^2) catchments, 3 mulched and 3 unmulched, in the 2020 Colorado Cameron Peak Fire burn scar. The objectives were to (1) quantify sediment volumes and spatial patterns of erosion and deposition on a catchment and channel scale, (2) compare geomorphic change to mulch coverage, vegetation cover, precipitation intensity, burn severity, and morphologic metrics, and (3) identify conditions in which mulch may be most appropriate based on findings. Initial drone surveys were gathered in the spring of 2022 shortly after mulching and were differenced to surveys collected in fall of 2022, capturing the erosional effects of a Colorado monsoon season within a 6.4 cm horizontal resolution DEM of Difference (DoD). Structure from motion (SfM) errors were thresholded out of the DoD to yield maximum and mean levels of detection at 14 cm and 5 cm respectively. Vegetation was filtered from the DoD by supervised classification of vegetation in the drone imagery. We found hillslope erosion dominated the sediment budget, with the mulched catchments eroding 141% more per area than the unmulched. A regression model suggested erosion to be most influenced by vegetation, hillslope length, and maximum 60-minute rainfall intensity. Channels were overall net depositional, and patterns of erosion and deposition in channels were controlled by changes in

slope and stream power as well as local morphologic metrics. Our analysis does not find a significant impact of mulch at the catchment scale especially when coverage is low (~22%) and highlights the importance of understanding catchment attributes and processes when making post-fire treatment decisions.

ACKNOWLEDGEMENTS

I want to thank all involved in the development of this research. This project was supported by the Coalition for the Poudre River Catchment, the City of Greeley, Colorado Water Conservation Board, and the USDA Agricultural Research Service, to which I extend my thanks. A big thank you to my advisor Peter Nelson for his steady patience and guiding thoughts throughout the project as well as my committee members Stephanie Kampf and Ryan Morrison for their encouraging words.

I am grateful for Johnny Murray, Cameron Turnbow, Aidan Cruz, and Maddie Rivera who helped in collecting field data, Phoebe White who helped in contributing code for the MRMS analysis, the CSU drone center for their teaching, and all reviewers who helped improve this paper. Lastly, I am deeply grateful for the friends who welcomed me into their life here in Fort Collins, and my family back home who cheered from afar.

TABLE OF CONTENTS

1. INTRODUCTION

As wildfires increase in severity, frequency, and extent, understanding how they affect catchments is vital for management decision making. Fires remove vegetative cover, decrease surface roughness, and increase soil-water repellency (Benavides-Solorio and MacDonald, 2001, 2005; Robichaud et al., 2000). Consequently, burned soils are highly susceptible to runoff and erosion, which can lead to flooding, debris flows, and sedimentation.

To mitigate these risks, post-fire treatments such as mulch may be applied to high priority burn areas. Mulching is one of the most common post-fire management techniques (Prosdocimi et al., 2016), as it provides immediate ground cover for exposed soil and protection from raindrop impact and overland flow (Foltz and Wagenbrenner, 2010; Robichaud et al., 2010a; Wagenbrenner et al., 2006). Furthermore, wood strand mulch is advantageous in that it can be derived from native forest materials, is easily transported to burned sites, and is durable. Robichaud et al. (2013a) found that wood strands reduced hillslope (~200 m^2) sediment yields by 79% and 96% for two different burn sites in Colorado during the first-year post-fire. On the plot scale (30 m^2), wood strands applied three years post-fire was shown to reduce runoff and sediment yields regardless of the volume of rainfall (Kim et al., 2008). Studies evaluating mulch beyond the hillslope scale are rare (Girona-Garcia et al., 2021), yet the few that have been conducted show mixed results. Fernandez et al. (2011) found no reduction in soil erosion for wood mulched swales (500 m^2) relative to untreated controls during the first-year post-fire. Prats et al. (2019) found an 84% decrease in soil loss on wood mulched swales (500-800 m^2) in the first-year post-fire while losses in the following years were more dependent on swale characteristics. Further field-studies are necessary to evaluate wood shreds on a catchment scale, since the larger scale involves a wider range of hydrologic processes and a greater level of

complexity. Mulched hillslopes are better protected against rainsplash, sheet flow, rilling, and gullying erosion, but downstream channel erosion and catchment deposition can continue to occur. Thus, upscaling sediment delivery from hillslopes may result in unreliable estimates of catchment scale sediment production (Moody and Kinner, 2006; Stoof et al., 2012).

Considerable advancements have been made in monitoring post-fire sediment movement. Early studies measured sediment yields using sediment fences or collection troughs constructed in the lab (e.g., Foltz and Wagenbrenner, 2010), on-site with a rainfall simulator (e.g., Benavides-Solorio and MacDonald, 2001; Johansen et al., 2001), or on-site under field conditions (e.g., Robichaud et al., 2013; Schmeer et al., 2018). These methods, however, are labor intensive and limit the volume of sediment that can be collected. In the past decade, remote sensing methods have become a prominent tool in topographic change detection. Effective change detection requires repeat surveys of an area of interest at relevant geomorphic time scales (Cook, 2017). Among survey methods, airborne Light Detection and Ranging (LiDAR) and Unmanned Aerial Vehicle (UAV) Structure from Motion (SfM) have become widely used in the geoscience community. Airborne LiDAR can collect topographic datasets over areas up to 1000 km^2, but its decimeter-scale uncertainty limits change detection to stream channels and valley bottoms where change exceeds uncertainty (Pelletier and Orem, 2014; Rengers et al., 2021). With recent advances in Unmanned Aerial Vehicles (UAV) and Structure from Motion (SfM) processing, UAV surveys have surpassed LiDAR in terms of cost and resolution. UAVs equipped with real-time kinematic (RTK) positioning systems can develop Digital Surface Models (DSMs) as fine as 5 mm with uncertainties around 3 cm (Alexiou et al., 2021; Nota et al., 2022). Surveys can also be flown with more convenience at desired time scales, such as leaf

off, at a fraction of the cost of LiDAR. Still, few studies have been done applying UAV-SfM to understand post-fire catchment response.

Accordingly, this study attempts to monitor post-fire erosion and deposition across six small catchments in the Cameron Peak Burn area using UAV-SfM photogrammetry. In 2020, the Cameron Peak Fire (CPF) burned over 830 km^2 of the Cache la Poudre basin, making it the largest wildfire in Colorado history. Mulching operations followed a year after the fire and created a unique paired comparison between adjacent catchments; three were mulched with wood strands and three were kept unmulched as controls. Shortly after mulching, we gathered repeat drone surveys of the 6 catchments to quantify change over a single monsoon season that occurred 2 years post-fire. The objectives of this study are to (1) quantify sediment volumes and spatial patterns of erosion and deposition on a catchment and channel scale, (2) compare geomorphic change to mulch coverage, precipitation patterns, contributing area, and morphologic metrics, and (3) identify conditions in which mulch may be most appropriate based on findings.

2. METHODS

2.1 Study Site

We selected six adjoining catchments, three mulched and three unmulched, to investigate the impacts of mulch on post-fire geomorphic response. The catchments burned in the Cameron Peak Fire, drain into Bennett Creek to the northeast, and range in size from 0.57-1.49 km^2 (Figure 1). Elevation ranges from 2342 m to 2779 m and mean slope ranges from 24.5% to 28.5%. The catchments burned to a comparable severity, mostly moderate with high severity patches surrounding the channels. The dominant vegetation in the area pre-fire included ponderosa pine (Pinus ponderosa), Douglas-fir (Pseudotsuga menziesii), and lodgepole pine

(Pinus contorta) as well as a diverse understory of shrubs and grasses (USGS, 2006). The underlying geology is primarily biotite granite and schist (USGS, 2018). Soils are classified as Cypher-Ratake families complex and Bullwark-Catamount families complex with frequent rock outcrops (Soil Survey Staff, 2022). The mean annual precipitation of the site ranges from 400 mm to 500 mm (PRISM Climate Group), characterizing the study site climate as semi-arid. Convective thunderstorms are common in the summer, while spring and fall tend to bring lower-intensity frontal storms. During winter months, snow is the predominant form of precipitation, and makes up approximately 40% of the annual precipitation (Colorado Climate Center).

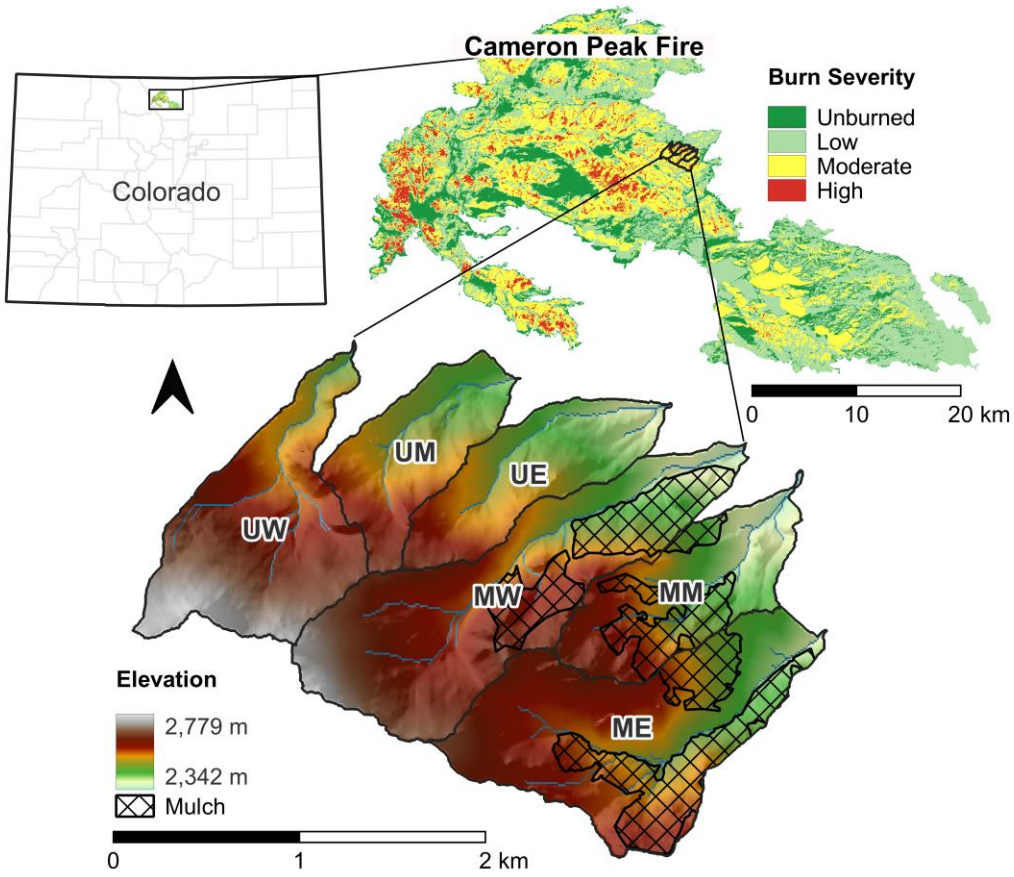

Figure 1. Location and burn severity of the Cameron Peak Fire (CPF) in Colorado with elevations and mulch coverage of the Bennett Creek catchments

The channels within each catchment are characterized by step pools in which large wood form the steps and sandy vegetated beds are upslope from headcuts. This pattern, shaped by the catchment topography, follows an aggradation, incision cycle up the channel. Streamflow for each catchment is low, relatively steady, and sourced by groundwater seeps and precipitation. Channels within the MM, UE, and UW catchments have been observed to run dry in the late summer.

Wood mulch was applied aerially to portions of the three easternmost catchments during late summer of 2021. Approximately 23%, 31%, and 33% of the Mulched West (MW), Mulched Middle (MM), and Mulched East (ME) catchments were mulched respectively at a coverage of about 22%, although the coverage was found to be inconsistent across the study area. Cover was measured within the mulch footprint by laying a 50 cm x 50 cm quadrat over a plot and taking 25 point measurements of mulch, soil, rock, wood, or plant at each 10 cm grid intercept. In total, 92 cover plots were measured along 12 diagonal line transects, resulting in 71 m spacing between individual cover plots.

Table 1. General catchment metrics for the Bennett catchments

Catchment	Contributing Area (km^2)	Elevation Range (m)	Mean slope (%)	Low Severity (%)	Moderate Severity (%)	High Severity (%)	Mulched Area (%)
UW	1.03	2454-2779	24.7	11	81	8	0
UM	0.57	2406-2652	24.5	11	74	14	0
UE	0.62	2369-2649	26.6	5	80	15	0
MW	1.49	2354-2759	27.7	15	74	12	23
MM	0.71	2342-2639	28.5	20	74	6	31
ME	1.37	2384-2681	25.9	18	71	11	33

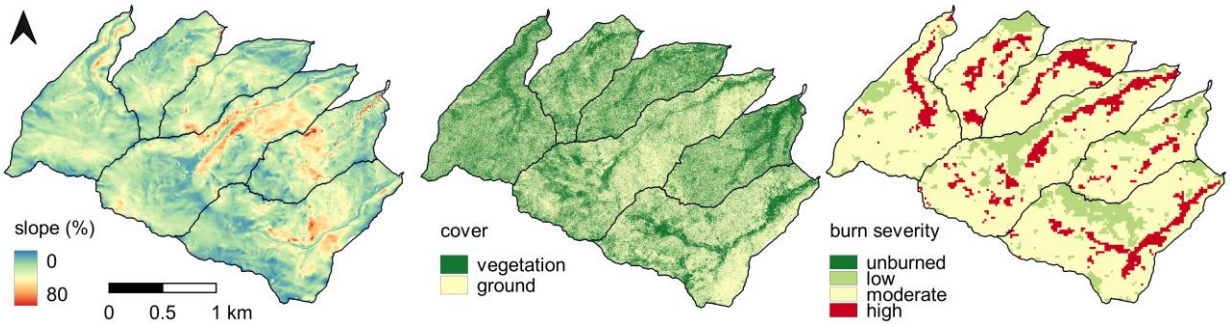

Figure 2. Catchment attributes show spatial patterns of slope, vegetative cover classified from the drone imagery, and burn severity post-fire

2.2 Data Collection

We collected imagery across the six catchments using a DJI Phantom 4 RTK drone during May and October of 2022. Surveys were done by autonomous nadir flight, and images were taken with a 1-inch 20MP CMOS mechanical shutter camera. Each image was geotagged based on the RTK base station and available satellites. The RTK base station was set over known coordinates from previous RTK-GPS surveys, and its coordinates were inputted into the drone pre-flight. Flights were programmed to operate under uniform parameters: terrain following mode allowed each photo to be taken 100 m above ground level (AGL) relative to an imported 10 m digital elevation model (DEM) in WGS84 coordinates. Photos were taken by distance with 70% horizontal and 80% vertical overlap, a 3:2 photo ratio, and an average metering mode. Prior to UAV flights, 54 GCPs were spray painted as Xs on boulders across the study site and surveyed with an RTK-GPS to further align and reference the DEMs. A channel cross section and longitudinal profile were also surveyed in each catchment to verify the UAV generated DEMs and track smaller in-channel geomorphic changes.

2.3 UAV-SfM Processing

We employed Agisoft Metashape to process the drone images into dense point clouds and digital elevation models (DEMs). The algorithms used by Metashape recognize identical features, or tie points, between the photos to stitch them together into a model. Our general procedure followed the photo alignment, GCP matching, and optimization guidelines from the USGS Structure from Motion Documentation (Over et al., 2021). Only easily identifiable GCPs were used in processing (24 total). Thus, we incorporated coregistration of the 2 surveys which has demonstrated nearly identical distribution of measured change compared to the classical GCP approach (Cook and Dietze, 2019). During alignment we loaded both surveys into a single chunk and checked images from one survey to act as a reference for the second survey. After these steps, dense point clouds, DEMs, and orthomosaics were generated. DEMs of 6.4 cm horizontal resolution were differenced to produce a DEM of Difference (DoD) for each catchment where negative change represents erosion and positive change represents deposition.

The DoD was further filtered to mask out errors and vegetation. Since horizontal errors were much smaller than vertical errors, we assumed their effects were negligible and did not incorporate them into the DoD error analysis. Vertical error was more substantial and includes both systematic and random error (James et al., 2020). Systematic error is associated with measurement accuracy and quantifies relative offsets between 2 surveys likely arising from flight design, in-camera image processing, and SfM post-processing (James et al., 2020; James et al., 2017a). Our DoDs were assessed visually and at control points to find little to no spatially uniform error suggesting no obvious systematic error.

Random error, associated with measurement precision, arises from SfM image processing such as tie point matching and optimization (James et al., 2020). Spatial random errors were

accounted for using a workflow by James et al. (2020) where precision estimates as XY points were extracted from Metashape for each DEM. Precision estimates for each DEM were gridded by Kriging into a raster of 6.4 cm resolution. We then propagated the DEM random errors to the DoD under the assumption that errors were Gaussian and independent between the two surveys (Brasington et al., 2003; Lane et al., 2003) where δ_{DoD} is the propagated DoD error and δ_{May} and δ_{Oct} are the random errors of the May and October DEMs.

$$\delta_{DoD} = \pm 1.96 \sqrt{\delta_{May}^2 + \delta_{Oct}^2} \quad (1)$$

To minimize the effect of random errors, we applied a 95% confidence threshold to the level of detection, so only cells with values outside of the 95% threshold were regarded as having real change. For example, if δ_{DoD} at a certain pixel was 8 cm, all change between -8 cm and +8 cm was regarded as having 0 change.

A visual check of the thresholded DoDs revealed that elevation change was greatly influenced by seasonal vegetation growth. Thus, we used the Semi-Automatic Classification QGIS Plugin (SCP) to classify vegetation from the drone imagery and filter it out of the DoD. SCP classifies ground cover by comparing pixel spectral characteristics based on RGB band combinations (Congedo, 2020). We identified 25-30 regions of vegetation and 20 regions of bare soil in each catchment's Fall imagery to be used as training input into the Maximum Likelihood classification algorithm. This algorithm calculates the probability distributions for each class, related to Bayes' theorem, and is one of the most common supervised classifications (Congedo, 2020). Its output classified each pixel of the imagery as vegetation or bare soil in the form of a binary raster (see Figure 2). We tested 100 random points over the output raster to calculate its accuracy. The raster was then multiplied to the DoD to neglect areas of vegetated cover.

2.4 Sediment Budget

Volumetric estimates of gross erosion and deposition were calculated by summing the DoD change multiplied by cell area. Our sediment budget explores erosion volume change on the catchment scale and both erosion and deposition volume change on the channel scale. Channelized zones, which included main channels and tributaries, were delineated manually according to orthomosaics and upstream contributing drainage area thresholds: tributaries represent all areas 10,000 - 100,000 m^2 and channels represent areas >100,000 m^2.

When calculating volume uncertainties, spatial correlation of the DoD error is likely to influence the results and should be considered (Anderson, 2019). Here we use statistical methods for propagating spatially correlated random errors presented in Rolstad et al. (2009) by converting each raw, unfiltered DoD to points and running a semi-variogram analysis. A spherical semi-variogram model with no nugget was generated using the ArcMap Kriging tool to yield the DoD's semi-variance and range. Volume uncertainty can then be calculated using the following error propagation formula (Rolstad et al., 2009):

$$\sigma_v = \sqrt{n} L^2 \sigma_{sc} \sqrt{\frac{\pi a_i}{5L^2}} \quad (2)$$

where n is the number of cells, L is the cell size, σ_{sc} is the square root of the semi-variance at the sill, and α_i is the fitted range. Finally, we multiply σ_{sc} by 1.96 for consistency in reporting estimates to the 95% confidence interval (Anderson, 2019).

2.5 Precipitation

Rainfall accumulation and intensity across the study site were monitored using NOAA Muti-Radar Muti-Sensor Quantitative Precipitation Estimates (MRMS QPE) and verified with 4

tipping bucket rain gages stationed in the Bennett catchments. After obtaining the gridded 1-km hourly MRMS data, a python script corrected the Multisensor 1 hour QPE by the radar only QPE and resampled the output to 1 min accumulation (Zhang et al., 2016). Daily precipitation was summed for each 1 km grid cell beginning from the day of the initial drone flight (10 May 2022) to the day of the final drone flight (29 October 2022) to yield total accumulation. A time series of 15-minute intensities for each cell was calculated from the 1 min QPE estimates and compared to a time series of 15-minute intensities for each tipping bucket gage. After verification, a spatial map of maximum 60-minute intensity estimates was generated from the MRMS data. We used maximum 60-min rather than 30-min or 15-min intensity values as 60-min intensity thresholds have been identified to separate rain storms that generated sediment delivery responses from those that did not (Wilson et al., 2018).

2.6 Catchment Scale Erosion Controls

A mix of catchment-scale and channel-scale controls operate to transport sediment throughout the catchments. To examine these controls, we analyze catchment-scale volumes and longitudinal channel change separately but acknowledge that the two are interconnected.

On the catchment scale, we calculated correlations (r) between erosion and predictor variables and used a bootstrap forest regression model to quantify drivers of erosion. A bootstrap forest or random forest model takes a nonparametric machine learning approach to fitting numerous predictors with potentially nonlinear relationships by creating decision trees based on random data subsets to determine an optimal model (Breiman, 2001; Zipper et al., 2021). We chose the bootstrap forest technique as it was relatively simple to run in JMP Pro, yielded a stronger predictive model than a multi-linear technique, and has relatively low risk of overfitting. Catchments were first delineated into hillslope sub-units of 5,000 – 50,000 m^2 using ArcHydro

Tools, and erosion volume was summed within each hillslope unit. In the model, the dependent variable was erosion volume divided by sub-unit area, and the predictor variables were mean slope, hillslope length (*L*), hillslope width (*w*), area, shape (categorical; i.e., convergent, divergent, planar), elevation range, maximum 60 minute intensity (MI_{60}), accumulated precipitation (*P*), mean burn severity (*dNBR*), fraction of the area mulched, fraction of the area with vegetation, and the SfM error raster. Predictor variables were sourced from our drone data, MRMS precipitation analysis, and BAER burn severity maps. Select variables such as normalized erosion, hillslope length, width, area, and slope were log-transformed to limit skew. Variables were evaluated for collinearity to find none highly correlated ($r > 0.85$). We then constructed the model in JMP using an 80% training and 20% testing data split, and measured model performance for both training and testing sets with R^2 and root mean squared error (RMSE) metrics. Because of the random sampling of the bootstrap forest technique, we ran the model 100 times and chose the model with the best performance to inform relative influence of each predictor variable.

2.7 In-Channel Sedimentation Controls

Within the channel, both positive and negative changes were examined based on the following metrics: slope, change in slope (Δslope), stream power, and change in stream power (Δstream power). A series of ArcMap tools and MATLAB scripts were used to determine channel centerlines for each DEM and extract slope, channel change, and channel widths at 1-meter intervals along the centerline. Given that the 6.4 cm DEMs depict such fine local detail, we resampled the DEMs to 1 m to calculate slope along the centerline. Topographic change was also resampled to take the maximum value across 1 m intervals. Positive and negative changes appeared to cancel out when binned into slope and stream power intervals. So, we implemented a

6 m average window for the slope, width, and change, as it was long enough to show patterns of change between the segments. Thus, Δslope was quantified by differencing 6 m segments where a positive change in slope represents a decreasing slope while a negative change in slope represents a steepening in slope. Unit stream power (ω), often used to predict erosion and deposition, is expressed as:

$$\omega = \frac{\gamma Q S_f}{w_c} \quad (3)$$

where γ is the specific weight of water (N m^{-3}), Q is discharge (m^3 s^{-1}), and S_f is the friction slope (m m^{-1}). In our analysis, we instead used the ratio of channel slope to width ($\frac{S}{w_c}$) as a proxy for stream power since continuous flow data were not available. Change in stream power was then computed similarly to Δslope, subtracting upstream and downstream 6 m segments.

3. RESULTS

3.1 Precipitation

MRMS estimated total precipitation to be highest over the western unmulched catchments while maximum 60-minute intensity was highest over the lower portions of each catchment (Figure 3). High intensity localized storms occurred over lower UM, UE, and MW which is corroborated by the on-site rain gages.

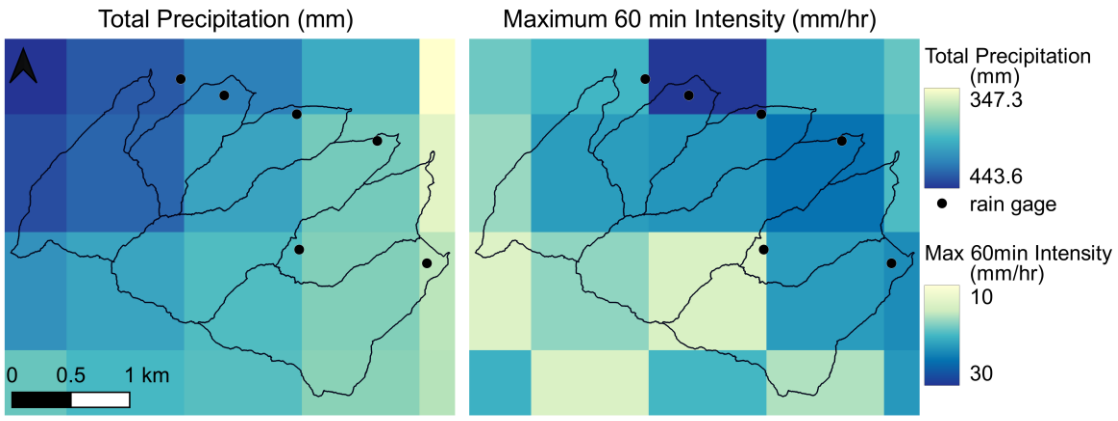

Figure 3. MRMS QPE over study period with field rain gage locations indicated

The tipping bucket rain gages inconsistently recorded rainfall for the period of study, sometimes skipping weeks of rainfall at a time. Only the UE gage recorded continuously, so the intensity of rainfall at the UE gage was compared to the MRMS estimates to verify radar use. Figure 4 plots the 15-minute intensity of the UE gage against the radar estimate for select rainfall events. Overall, MRMS tends to overestimate intensity and accumulation compared to the gage; however, it is not consistent event-by-event. For example, MRMS predicts more than double the intensity tracked by the gage on 7/16, while it underestimates the intensity tracked on 7/24 (Figure 4). A large event on 7/28 indicates similar intensities for both the gage and MRMS estimate. In other events, MRMS overestimated values for high-intensity storms (>40 mm/h) and underestimated values for low-intensity storms (<10 mm/h). Given that storms in the Colorado Front Range are often very localized and intense, a resolution of 1 km horizontal cannot predict the intensity and accumulation at an exact location such as a gage. Still, the overall pattern of intensity tracks with the gage, indicating the MRMS QPE provides a reasonable description of spatial patterns of precipitation across the Bennett catchments.

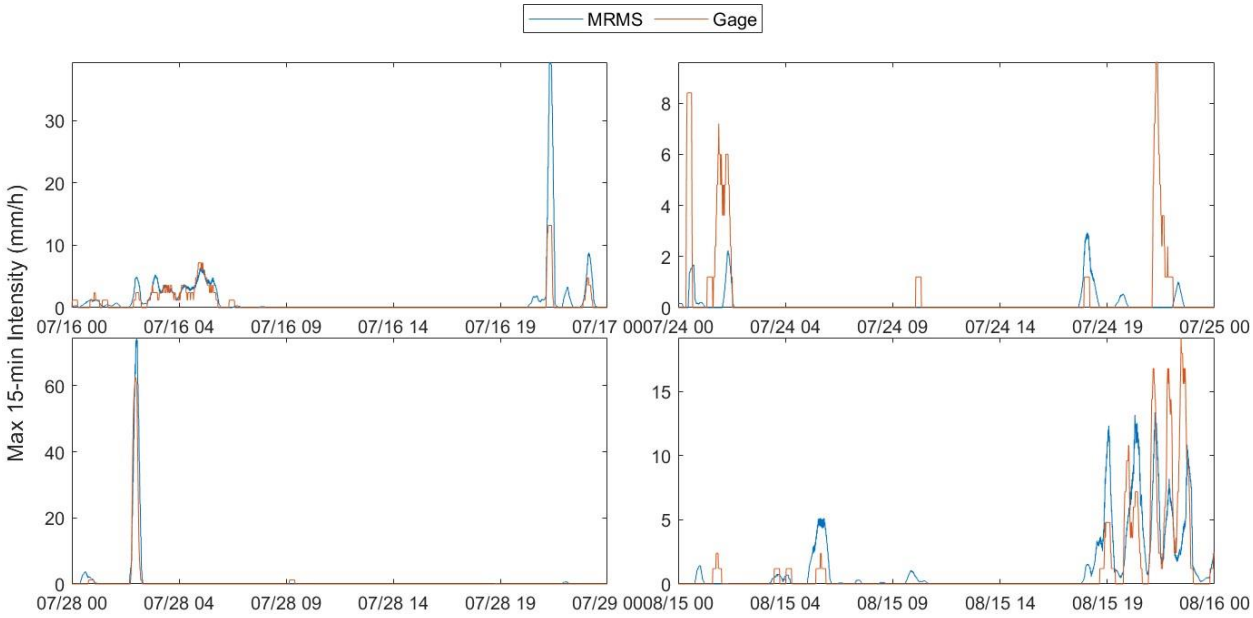

Figure 4. Event based 15-minute intensities verify the use of MRMS estimates with the UE rain gage

3.2 Level of Detection and Topographic Change

Our SfM error analysis yielded spatially distributed levels of detection with the maximum and mean levels of detection shown in Table 2. The errors did not randomly distribute in space; high errors concentrated in the valleys where vegetation was present, whereas bare hillslope errors were usually smaller. The MM survey experienced widespread shadow errors, so we decided to neglect MM results in this analysis.

Table 2. Maximum and mean vertical and horizontal errors for each catchment

Catchment	GCPs used	Max horizontal error (m)	Mean horizontal error (m)	Max vertical error (m)	Mean vertical error (m)
UW	7	.039	.006	0.13	.042
UM	4	.039	.007	0.14	.043
UE	2	.036	.007	0.12	.050
MW	6	.038	.006	0.13	.044
MM	2	.056	.011	0.16	.067
ME	4	.043	.008	0.14	.052

Due to such fine resolution and vegetation signals, DoD change at the catchment scale is difficult to view (Figure 5a). Zooming in to the hillslope scale, we find select hillslopes with widespread erosion and rilling, for example a hillslope in MW (Figure 5). The greatest vertical topographic change takes place within the channel: up to 2.5 m of erosion and 0.75 m of deposition (Figure 6). Incision and aggradation alternate along each channel with erosion occurring at meander bends and deposition occurring upon widening. Hillslope tributaries are marked by straight erosional pathways converging downstream to the main channels.

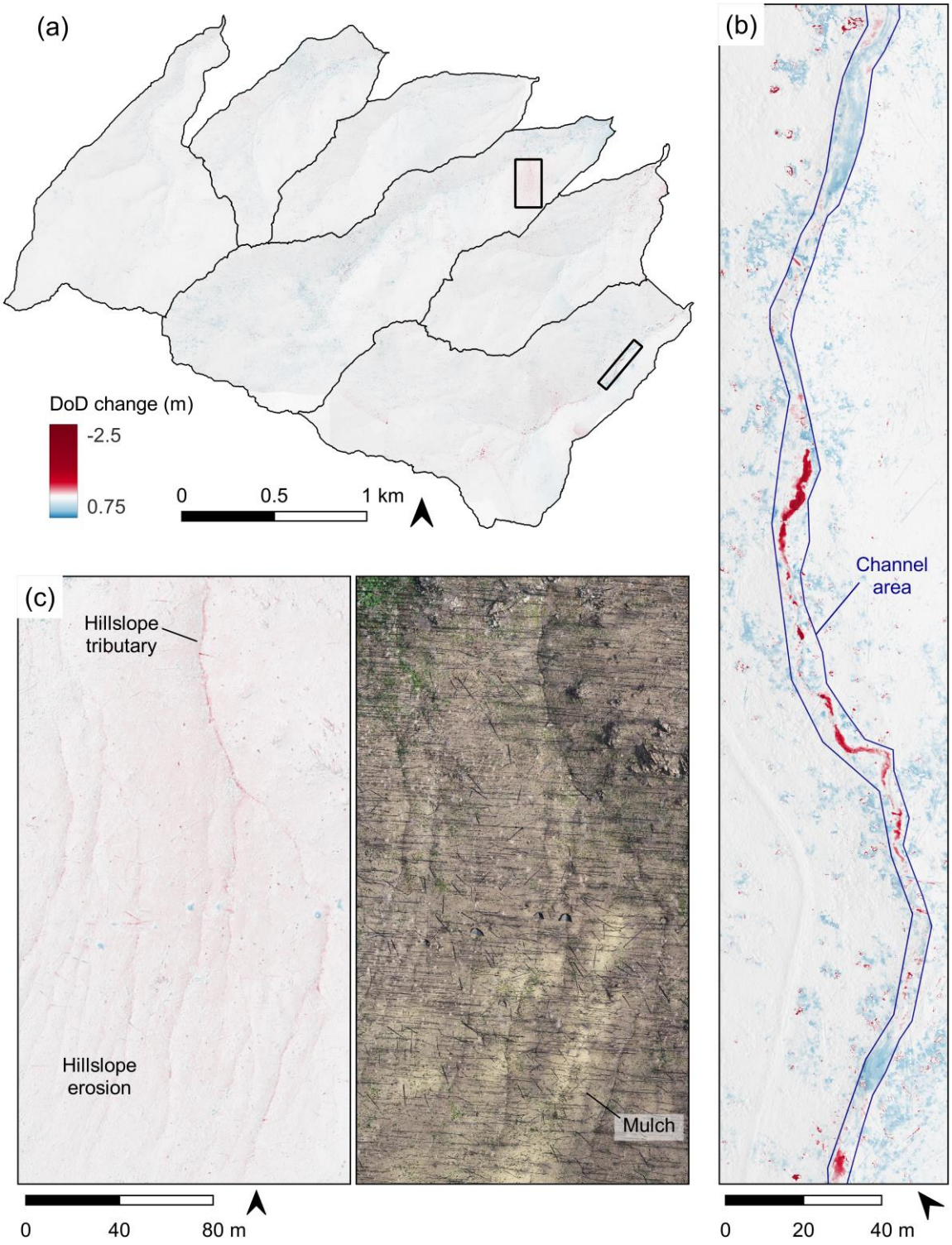

Figure 5. DoD. a) Topographic change across the entire study area. Boxes show locations of detailed maps in (b) and (c). b) Zooming in to the channel scale, incision and aggradation alternate upstream. c) Hillslope scale changes are detected where overland flow and rills become a tributary despite upslope mulch coverage.

Figure 6. The greatest vertical change occurred within the channels. Left: a headcut in ME precedes 2.5 m of vertical incision. Right: a reach in UE displays ~0.3 m of aggradation.

Despite efforts to filter vegetation, the DoD displays patches of positive change from summer vegetation growth (Figure 5). Testing the SCP classification raster at 100 random points indicated a 77% accuracy in identifying vegetation versus ground points. The vegetation signals remaining in the DoD interfered with our ability to quantify deposition on the catchment scale accurately. Thus, we only quantify erosion volumes over the catchments. We found erosion to be less associated with vegetation since our Spring survey was flown directly after snowmelt and little vegetation was available to die off and appear as erosion. Delineated channel zones were relatively free from vegetative effects, so we focus analysis on channel change and erosion across the catchment.

3.3 Sediment Budget

Estimated sediment volumes show the mulched catchments had a greater erosional response compared to the unmulched catchments. Hillslope yields dominated the sediment

budget over channel erosion with hillslope erosion accounting for 90-92% of erosion for all catchments except UE where hillslope erosion accounted for 50% (Table 3). Channels made up 1-2% of each catchment's total area. After normalizing the volumes by area (Figure 7a), the mulched catchments eroded 141% more than the unmulched catchments. Deposition at the catchment scale was not calculated due to widespread vegetation growth that could not be filtered accurately. Channels were overall net depositional and acted as sinks for the hillslope sediments. The upper portions of ME, MW, and UW were depositional whereas the lower portions of UE and UM were depositional. Erosion volumes in the channels and tributaries indicate UE had the most sustained channel erosion for its area with the mulched catchments experiencing slightly less. Channel response was variable with respect to several factors such as slope, stream power, and their downstream change and are explored more in Section 3.4.

Table 3. Sediment volumes for each catchment

	UM	UW	UE	MW	ME
Gross erosion (m^3)	-1546 (±1288)	-1276 (±1384)	-841 (±448)	-5955 (±3677)	-5775 (±2346)
Erosion in channels (m^3)	-122 (±324)	-102 (±469)	-423 (±370)	-469 (±1088)	-583 (±748)
Deposition in channels (m^3)	698 (±518)	603 (±627)	488 (±256)	1704 (±1146)	550 (±563)

3.4 Catchment Scale Erosion Controls

Sediment yields varied between the catchments and exhibited complex behavior with respect to slope, mulch, and upstream contributing drainage area. All catchments had their greatest fraction of area within the 20-30% slope range. Yet, the greatest erosion for the unmulched catchments occurred in the low slope range of 10-20% (Figure 7c). The unmulched catchments had few areas with slopes above 40% (<5% of total area) as shown in Figure compared to MW and ME (18% and 13% respectively). MW and ME experienced more erosion

per area in the high slope range of 30+% even with many of the steep slopes mulched. Compared to total catchment erosion, mulched areas in ME eroded less per area while mulched areas in MW eroded more per area (Figure 7b). All catchments exhibited an increase in eroded sediment volume with an increase in contributing area, although volumes between the catchments are not constrained (Figure 7c). Unmulched volumes were generally less than mulched volumes for similar contributing areas. The volume-area curve (Figure 7c) for ME is significantly steeper, even for small areas. The MW curve follows the UW and UE curves until it hits a contributing area of 10^6 m^2 where it steepens considerably.

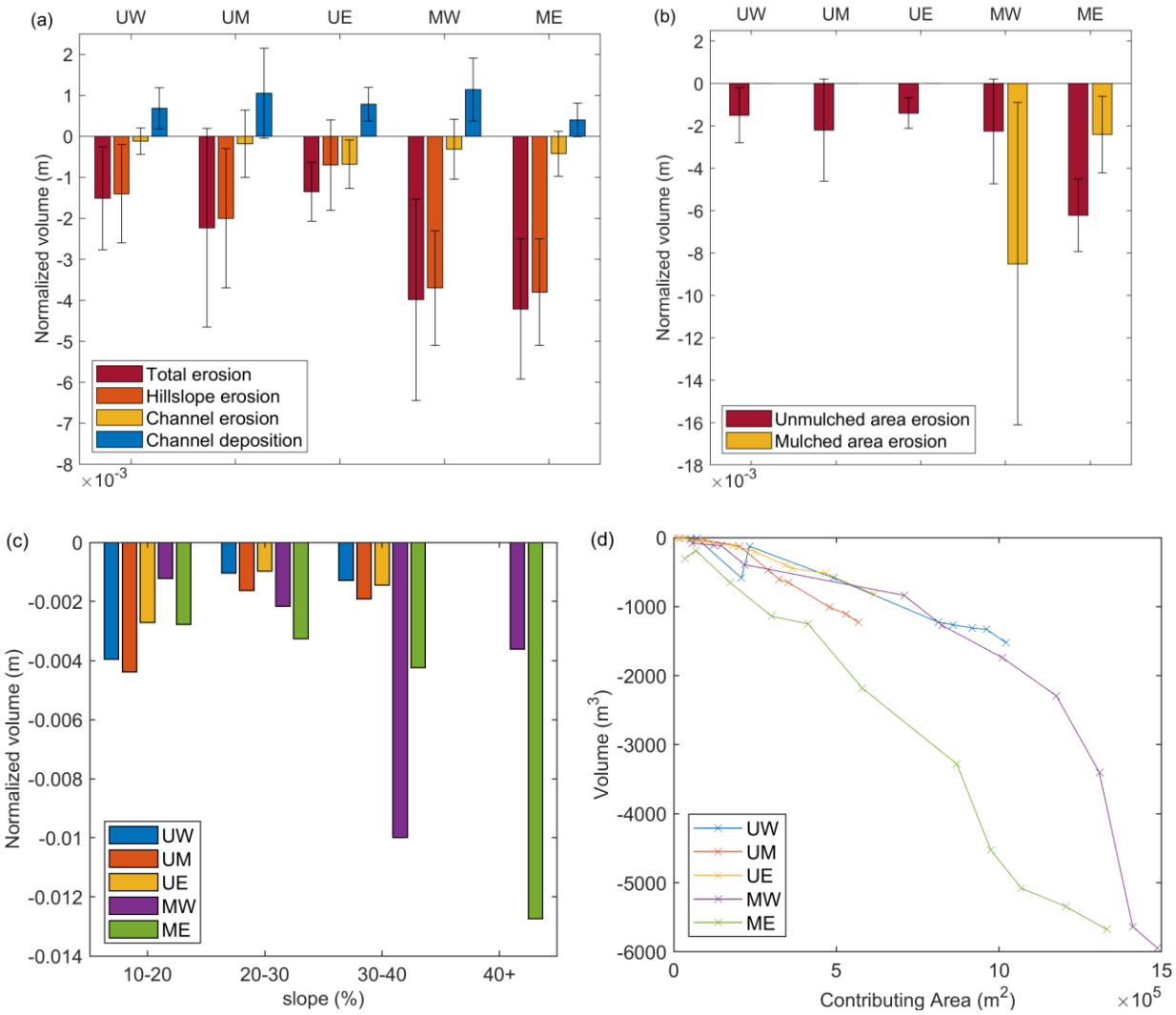

Figure 7. a) Sediment volumes divided by catchment area. Positive values indicate deposition, negative values indicate erosion, and verticals bars indicate uncertainty. b) Mulched and unmulched erosion divided by catchment area mulched or unmulched. c) Normalized erosion volumes binned by slope. d) Gross catchment erosion as a function of contributing area.

The bootstrap forest model of hillslope erosion performed adequately and obtained a training dataset R^2 and RMSE of 0.762 and 0.239 m respectively (Figure 8). The resulting model used 326 observations, 9 decision trees, and sampled 9 of the 11 terms per split. Notably, the testing dataset produced a weaker performance of R^2 = 0.370 and RMSE = 0.435 m. We,

however, do not plan to use the model for predictive purposes and analyze its performance solely to understand drivers of erosion.

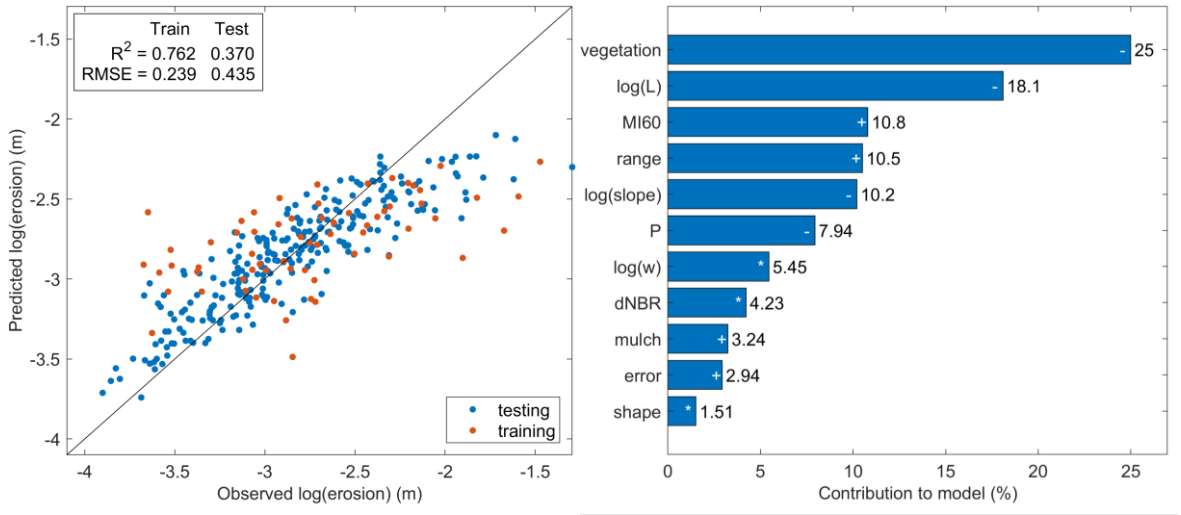

Figure 8. Bootstrap forest model performance shown as predicted vs. observed erosion. A 1:1 line is shown for reference (left). Component contributions are listed in order of contribution and "+" indicates a positive Pearson correlation to erosion, "-" indicates negative correlation, and "*" indicates insignificant correlation (right). For partial dependence plots with a more complete variable-response relationship, see Figure 10.

The resulting model identified vegetation, hillslope length, and maximum 60-minute rainfall intensity as top drivers of erosion (Figure 8). Vegetation and hillslope length contributed to the model substantially, although maximum 60-min intensity, elevation range, slope, and accumulated precipitation also played a significant role. Burn severity (*dNBR*) and hillslope width contributed somewhat to the model, and mulch, error, and shape contributed little. No one variable dominated the component analysis, least of all mulch, which highlights the complex feedbacks and processes between predictors occurring at the catchment scale. By the correlation matrix (Figure 9), vegetation was negatively correlated with erosion, hillslope length weakly negatively correlated, and MI_{60} weakly positively correlated.

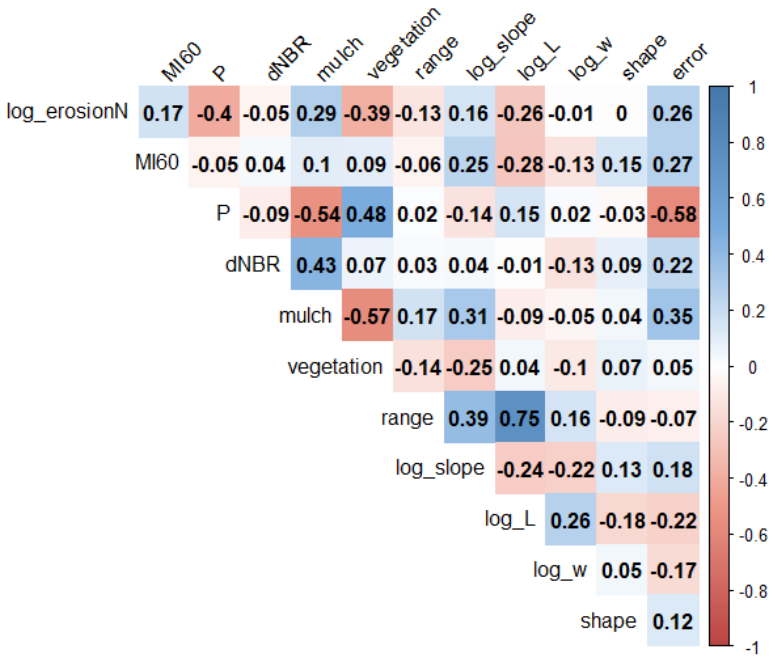

Figure 9. Pearson correlation matrix showing the relationship between predictor and response (log_erosionN) variables. No coefficient exceeds 0.85, so all predictors were used in the model.

Since random forest models capture nonlinearities, the model output does not give a direct relationship between variables, rather variables build upon each other to give a response (Breiman, 2001). Thus, partial dependence plots give a more complete impression than Pearson correlation coefficients. Our partial dependence plots (Figure 10) showed erosion to consistently decline with increasing vegetation.

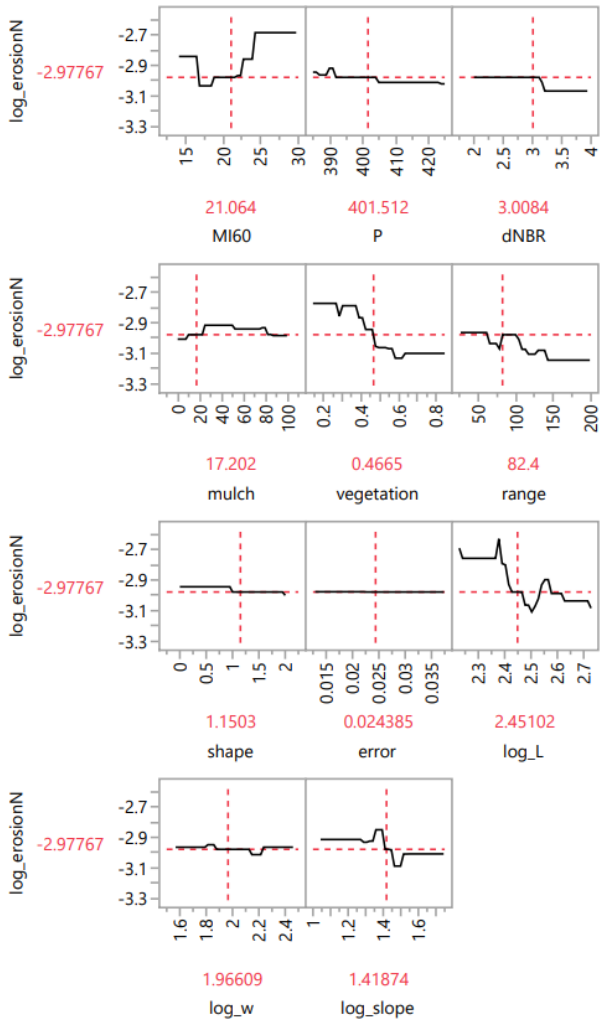

Figure 10. Partial dependence plots for the bootstrap forest regression model show a nonlinear predictor-model response relationship more informative than Pearson correlations. For all plots, the y-axis indicates volume of erosion divided by area and the x-axis indicates predictor values

Erosion fluctuated with different hillslope lengths increasing with length up to ~240 m and then generally decreasing for hillslopes exceeding 240 m. Surprisingly, the partial dependence plot and correlation matrix showed a slight decrease in erosion with increasing accumulated precipitation while the MI_{60} partial plot showed an increase in erosion for intensities above 17 mm/hr. The partial plot and Pearson coefficient agree for range indicating a negative relationship to erosion. Hillslope length was more correlated with elevation range, and

elevation range follows the same length-erosion relation. Plotted erosion fluctuated with increasing slope although the correlation indicates a positive relationship between slope and erosion. The relationship between erosion and error differed between the partial plots and Pearson coefficients; erosion did not change with increasing error, while the Pearson correlations indicated a weak positive relationship. Despite this discrepancy, the component contribution of error confirmed that the detected erosion was not primarily a result of data collection and processing errors.

3.4 In-Channel Sedimentation Controls

Figure 11 shows erosion in the channels is generally higher where slope increases in the longitudinal profile. This trend is further mapped in Figure 12, which plots mean change for slopes binned into 0.1 m/m intervals and stream power binned into 0.5 m^{-1} intervals. Here we see a slight negative relationship between slope and topographic change, although a steep slope or high stream power did not always indicate erosion. Change in slope and stream power also show an approximate positive linear relationship. Positive change in slope indicates concavity in the channel and often leads to deposition; while negative change indicates convexity, or a steepening in slope, and leads to erosion. Changes in sediment transport occur when slope or stream power changes, which explains the sustained erosion in the less variable UE channel. Visual observations reveal a change in slope or stream power to drive downstream change often beyond the 6 m sampling interval. Thus, the graphs still show scatter, more so in the Δ S/w figures.

Other sources of variability include discontinuities within the channel such as in-stream wood, tributary junctions, channel planform, vegetation, and local geomorphic effects. Points of greatest incision in the mulched catchments occurred in confined valleys where eroding hillslopes met the channel (500 and 800 m upstream in ME; 100 and 500 m upstream in MW;

Figure 11). Valley confinement in UE and UM was observed visually in the headwater reaches where sustained incision was measured. The lower reaches in UE and UM had low gradients, fine deposits, multiple flow paths, and well-established vegetation, all factors encouraging deposition. Vegetation acted to both confine and obstruct the channel, leading to incision or multiple flow paths. Variable planform such as bends allowed erosion; and widening, deposition. Channel spanning logs often produced erosion upstream or downstream of the structure. These channel specific interactions highlight the complex sediment connectivity between hillslope-channel linkages.

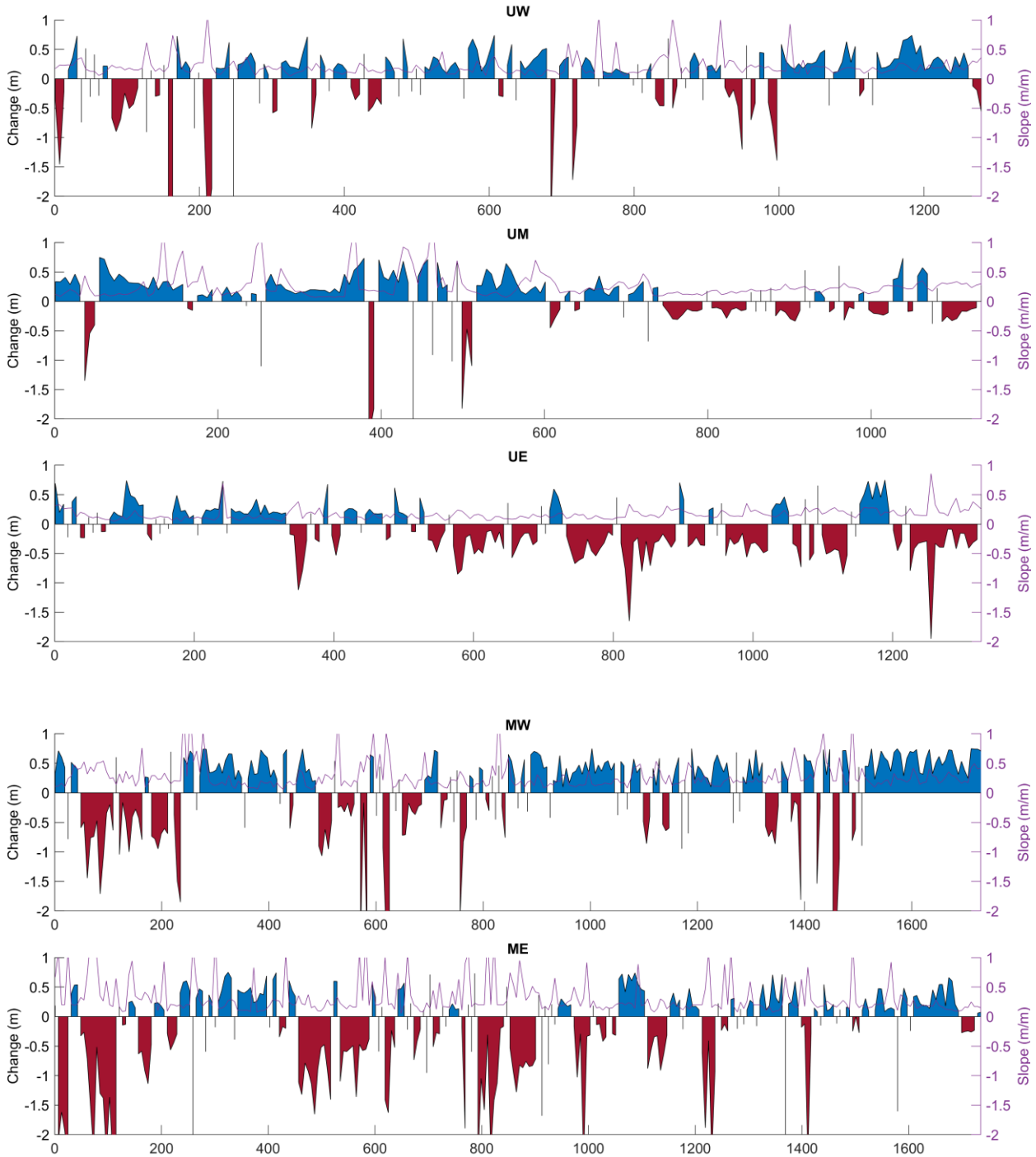

Figure 11. Erosion and deposition along each catchment's longitudinal profile as a function of distance from the outlet (primary y-axis) as well as the local slope along the longitudinal profile (secondary y-axis). Change and slope were resampled with a 6 m average window.

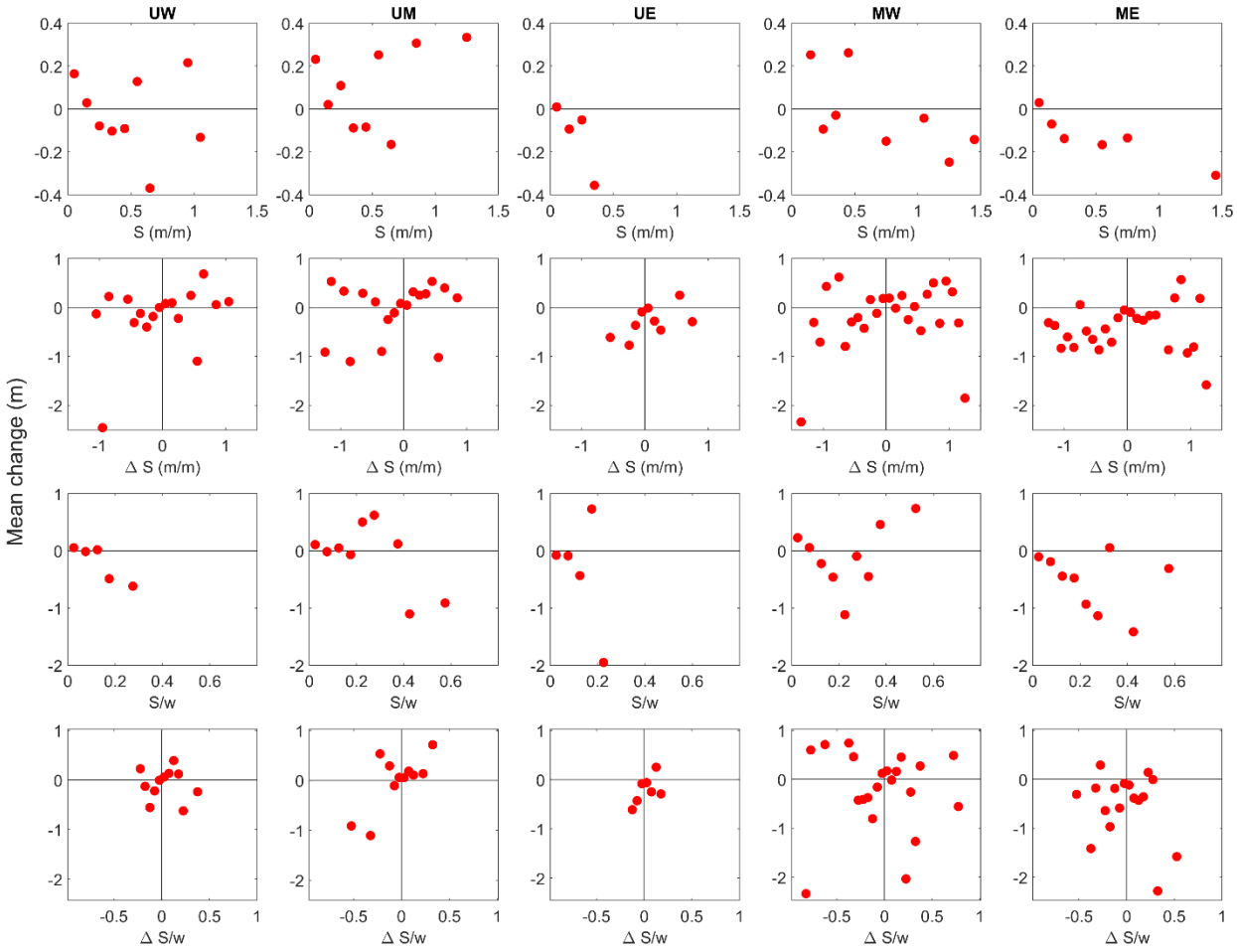

Figure 12. Topographic change in channels over 6 m intervals is binned into slope (S) intervals of 0.1 m/m and stream power (S/w) intervals of 0.5 m^{-1} intervals to highlight the relationship between change, slope, and stream power. Despite scatter, all 4 metrics seem to affect change with S and S/w showing a negative relationship and ΔS and Δ S/w showing a positive relationship. The graphs show MW to have the largest range in slope and UE to have the smallest range.

4. DISCUSSION

4.1 Sediment Redistribution Processes

Our findings demonstrate that the bulk of the erosion came from hillslopes while deposition occurred in the low-gradient reaches of the channels. Channels were net depositional, and we were unable to calculate sediment exported out of the catchment due to our challenges

filtering vegetation. Prior LiDAR studies also found hillslope yields to dominate catchment erosion (Rengers et al., 2021; Pelletier and Orem, 2014) but recognize that catchment size strongly influences sediment delivery. According to Rengers et al.'s (2021) slope-area curve, sediment yield increases linearly with contributing area for catchments of our size 0.5-1 km^2. At this size, Rengers et al. conclude fluvial processes dominate the channel network, and more eroded sediment passes through the channel than is deposited. Given our magnitude of erosion, we can trust that each of our study catchments exported volumes of sediment downstream despite channel deposition. Likely, volumes exported correlate in magnitude with catchment gross erosion, although the development of alluvial fans at the base of UE and UM and differing catchment attributes may suggest differences in predictions.

4.1.1 Model Predictor Response

Our bootstrap forest regression results showed that erosion volumes were primarily driven by vegetation, hillslope length, and precipitation intensity. Pearson coefficients between erosion and predictor variables found weak or negligible correlations, so we also use partial dependence plots given by the bootstrap forest model to better understand nonlinear predictor-response behavior. Erosion fluctuated with hillslope length; increasing up to 240 m length, and declining for longer slopes. This nonlinear trend follows the relationship assumed by the Universal Soil Loss Equation (USLE) which posits sediment yield to increase with slope length up to 120 m or up to 300 m in the case of the Revised Universal Soil Loss equation (RUSLE) (Wischmeier and Smith, 1978; Renard et al., 1991). Disturbed WEPP, a physically based model, indicates that erosion in dry climates increases with slope lengths up to 200 m and then declines after 250 m (Miller et al., 2011). At longer lengths, concentrated channelized flow dominates over rainsplash, sheetwash, and shallow rilling. Schmeer et al. (2019) found an overall decrease

in sediment yield with slope length for a study site like ours and notes the complexity of erosion and deposition along flow paths at larger spatial scales.

The direct influence of vegetation and precipitation intensity is corroborated by past studies that claim ground cover and rainfall intensity are two of the dominant controls on the amount of sediment generated after wildfire (Wagenbrenner et al., 2006; Robichaud et al., 2013a; Schmeer et al., 2018). Vegetation regrowth explains why sediment yields drastically decline after the first years post-fire. It reduces rainsplash erosion and increases the rainfall intensity threshold that allows overland flow to concentrate into rills, mitigating upslope erosion processes (Robichaud et al., 2013b).

Our study found rainfall intensity rather than total precipitation to be an important control on erosion response. There is consensus in this finding (Moody and Martin 2001; Robichaud 2005; Wischmeier and Smith; 1978), although total precipitation was surprisingly negatively correlated with erosion and showed a slight negative trend in the partial plots. This may indicate an error in the MRMS precipitation data. On the other hand, intensity, which was also derived from MRMS data, behaved as expected and was verified for various events with a rain gage (Figure 4). The negative correlation may be due to variable interaction, as total precipitation was correlated with vegetation.

Slope, elevation range, and burn severity have been proven to play a key role in erosion (Benavides-Solorio and MacDonald, 2005; Benavides-Solorio and MacDonald, 2001). Slope was weakly positively correlated with erosion while range was weakly negatively correlated with erosion. This opposition is most likely due to the variable interaction. Elevation range was highly correlated with hillslope length and acted similarly. Slope was negatively correlated with vegetation which confirms it to be a main control in vegetation recovery. Contrary to other

studies, burn severity had a slight negative relationship with erosion. Burn severity maps indicated greatest severity within valley bottoms, which suggests a drastic change in vegetation cover pre and post fire (BAER, 2020). Despite the high burn severity in valley bottoms, we found valleys to be more depositional than erosive, and so we see the negative relationship given in the model.

We found it important to include our spatial error map in the model to understand its relative influence on our calculated erosion volumes. Given that errors were propagated and thresholded out to a 95% confidence interval, areas with high errors had a coarser level of detection. So, we expect to find less change where errors are high. The partial plot displays no real relationship between erosion and error. Pearson coefficients, however, show a weak positive correlation between error and erosion. We do accept that errors play a role in our findings, specifically 2.94% of the regression model results, but this relatively low contribution of error in the prediction model verifies that the detected erosion wasn't primarily a result of erroneous change.

We emphasize that the model found significance in all predictor variables and the sediment yield data exhibited wide variability. Our model testing performance was relatively weak. For this reason, we do not report a sediment yield prediction equation. Other studies report similar variability, and published empirical models seek to predict sediment yields within an order of magnitude when applied in the right setting (Rengers et al., 2021; Pelletier and Orem, 2014; Nyman et al., 2020, Gartner et al., 2014). The variability is likely due to small-scale spatial heterogeneity that is hard to measure with predictor variables and compare between study sites. For example, Benavides-Solorio and MacDonald (2005) found soil water repellency and texture, variables not measured in this study, explained 77% of the variability in sediment production

rates at very small scales. More variables such as erosivity, soil erodibility, infiltration capacity, and ground cover metrics such as litter and rock could be added to the model to attain better prediction performance.

4.1.2 In-Channel Sedimentation Controls

Channel response was no less complex than hillslope response and has been proven to be dependent on site-specific interactions (Shahverdian, 2015; de Vente and Poesen, 2005). Patterns of erosion and deposition within our channel networks were somewhat explained by slope and stream power but showed high irregularity. A change in slope or stream power often marked a change in sediment transport, although tributary inputs, hillslope confinement, vegetation, large wood, and channel planform likely also regulated the transport. Previous studies have highlighted the challenges predicting channel response even when lateral inputs and sediment delivery rates are known due to reach morphology and the timing and magnitude of flows (Shahverdian, 2015; Eccleston, 2008; Legleiter et al., 2003; Lane et al., 2008). Additionally, channel inputs and response are episodic, and our study does not capture change after discrete events but instead shows an accumulation of many episodic changes. Furthermore, we measured change during the second year post-fire when sediment supply within the channels was already high, and channel erosion may have reflected incision through deposits left from the year prior. As the channels move through stages of geomorphic sensitivity based on time since fire and episodic activity, our ability to determine statistically significant relationships is confounded.

4.2 Evaluation of Mulch

The results of this study suggest that mulch had little impact on hillslope erosion at the catchment scale. Our SfM imagery showed the mulched catchments experienced the most

erosion per area, but they also had higher slopes and less established vegetation than the unmulched catchments as well as numerous other differing factors. Even so, our regression model indicated mulch to have the least influence on erosion after shape. Despite the number of studies proving the effectiveness of mulch at hillslope and smaller scales, our results are not unforeseen. Fernandez et al. (2011) found a 45% coverage of wood strand mulch to be ineffective in reducing soil loss on an inclined 500 m^2 slope relative to an untreated control. Other researchers found mulch to be effective on the plot scale but much less effective on larger scales up to a catchment (Robichaud et al., 2013b; Hubbert et al., 2012). Researchers have suggested that at least 60% cover is needed to reduce post-fire hillslope erosion rates (Robichaud et al., 2000; Orr, 1970; Foltz and Copeland, 2009). Our mulch coverage of ~22% pales in comparison to the suggested coverage. Though 22% coverage may be an incremental step towards retaining sediment on hillslopes, it does not reach the threshold needed to significantly reduce sediment yields. We attribute such low coverage to aerial mulching application. In our experience, we observed it difficult for helicopters to drop wood mulch in the desired locations to the desired coverage. Coverage also declined over time due to mobilization during high-intensity events, and mulch was found deposited in tributaries and caught behind felled logs. Declining coverage over time is not necessarily unfavorable as studies show sediment yield to decrease each year after the fire (Schmeer et al., 2018; Robichaud et al., 2013b); thus, mulch would no longer be necessary. Given the widespread recovery of vegetation at our site, our results may have differed if we had evaluated mulch during the first year post-fire.

The decision on where to apply mulch is typically based on burn severity, slope steepness, geologic characteristics, and downstream values at risk (Cannon et al., 2001; Robichaud, 2000; Rathburn et al., 2018). In the case of the Bennett catchments, mulch was

applied to steep, severely burned hillslopes to mitigate large sediment fluxes into a downstream drinking water source, the Cache La Poudre River. Given our findings on mulch effectiveness, we suggest if mulch is used, it be on steep hillslopes where sheetflow dominates with little to no ground cover promptly after burn to mitigate small scale sediment yields. For catchment scaled restoration, we recommend future efforts to be directed towards promoting deposition in valley sinks and vegetation recovery on the hillslopes. Catchment attributes, climate, and downstream catchment connectivity should also be evaluated to predict the risk of debris flows and sediment delivery. Lastly, physical complexity in streams should be promoted as it often allows for the greatest sediment recovery and watershed resiliency (Rathburn et al., 2018).

4.3 Data Accuracy Assessment

The success of topographic change studies is fully dependent on separating real change from apparent change due to error. In this study, we minimize survey errors, both horizontal and vertical, to reveal actual change. We neglected horizontal error and vertical systematic error since estimates were much smaller than vertical random error. This may underestimate the DoD error. Uncertainty was then dominated by vertical random error, which we propagated and applied a confidence level to threshold the DoDs. Anderson (2019) found that thresholding is crucial when quantifying gross changes but has potential to degrade net change estimates and associated uncertainty. Given that we are most interested in quantifying total erosion volumes for the catchments, we use error thresholding but acknowledge that thresholding loses significant measurements in the process. Our average uncertainties of 5 cm and maximum uncertainties of 14 cm limit us in detecting processes such as rainsplash, sheetwash, and shallow rilling. Even so, our levels of detection are average for similar SfM studies and low for LiDAR studies (de Haas

et al., 2021; Dai et al., 2022; Pelletier and Orem, 2014) and give us the resolution needed to understand erosion at the hillslope scale.

Separating sediment movement from ground change was also a challenge. Logs migrating downslope would appear as a line of erosion followed by a line of deposition on the DoD. A sprouting shrub would appear as a patch of deposition. Although a 6.4 cm resolution DoD is helpful in showing fine in-stream bed movement, it can be overwhelming in making sense of change at the catchment scale. Because upland catchments are mostly hillslopes, potentially erroneous values can collectively sum to a large proportion of change. Classifying vegetation using SCP allowed us to filter most of the erroneous change due to vegetation, downed trees, and shadowing, although it was not perfect. The imagery showed vegetation to be widespread in our Fall survey in contrast to our Spring survey, although it was seasonally brown and dying. This made separating vegetation from bare soil a challenge for SCP. If we trained SCP using a survey flown mid-summer when vegetation was green, SCP would have performed better, perhaps to the point of identifying only real deposition. Even with advanced vegetation removal methods, vegetation can act as a riparian buffer and obscure sediment deposited within it, making it difficult to quantify depositional yields from the DoD along the channels. Despite these challenges, we can be confident in our sediment yields for 5 reasons: (1) thresholding the DoD based on spatial error estimates is a conservative measure to filter out erroneous values; we believe that in thresholding out significant change, the erroneous change present beyond the level of detection is compensated for; (2) we were able to classify vegetation to a 77% accuracy and filter out most of its erroneous change; (3) we calculate and include large uncertainty volumes (4) we use a statistical model to verify our hillslope erosion and its drivers are comparable to

those found in past erosion studies; and (5) we do not analyze deposition or the MM catchment, which was visually clouded with errors.

Our experience processing SfM imagery indicates the need to collect surveys efficiently and as soon as possible following a fire, collect elevation surveys at the same time each year during leaf-off as well as a vegetation survey, and visually investigate the study site to verify the drone imagery from a ground perspective. As SfM processing and machine learning advances, vegetation and error removal will become more seamless and increase our confidence in ground change. New technologies such as PPK processing and fixed-wing drones will allow larger catchments to be flown and analyzed without ground control. Our results are a step forward in cost-effectively identifying and predicting sediment redistribution post-fire and ultimately helping guide catchment managers in decision-making.

5. CONCLUSION

In this study we used repeat drone surveys to analyze the catchment scale effects of mulch on sediment movement 2 years after the 2020 Cameron Peak Fire. Our first objective was to understand the spatial patterns of erosion and deposition by quantifying sediment volumes across the catchment and within the channel. We found erosion to be primarily sourced from hillslopes, while channels acted as depositional sinks. The mulched catchments eroded more per area than the unmulched catchments likely because they had larger areas of steep slopes. We were not able to measure deposition on the catchment scale due to challenges filtering vegetation growth. Our second objective sought to determine the drivers of change within the catchments and channels. Vegetation, hillslope length, and precipitation intensity were the most influential variables in the regression model, although all predictor variables had some influence on the model highlighting the complex relationship between catchment attributes. Within the channels,

physical complexity such as changes in slope and stream power drove incision and aggradation. Our last objective was to evaluate mulch and propose conditions in which it is useful. We found wood strand mulch at a coverage of ~22% to have little to no influence at the catchment scale. If mulch is to be used, it should be applied on steep hillslopes less than 250 m long, with low vegetative cover directly after fire. This study highlights the importance of understanding catchment processes when making post-fire treatment decisions. We find quantifying change using UAV-SfM techniques to be a progressing yet effective way to understand post-fire sediment redistribution and treatment priority. Future research should focus on mapping change over larger catchments and training algorithms to detect and filter vegetation and erroneous change.

REFERENCES

Alexiou S., Deligiannakis G, Pallikarakis A, Papanikolaou I, Psomiadis E, Reicherter K. (2021). Comparing High Accuracy t-LiDAR and UAV-SfM Derived Point Clouds for Geomorphological Change Detection. *ISPRS International Journal of Geo-Information*. 2021; 10(6):367.

Anders, N., Valente, J., Masselink, R., & Keesstra, S. (2019). Comparing filtering techniques for removing vegetation from UAV-based photogrammetric point clouds. Drones, 3(3), 61.

Anderson, S.W. (2019). Uncertainty in quantitative analyses of topographic change: error propagation and the role of thresholding. Earth Surf. Proc. Land. 44 (5), 1015–1033.

BAER (Burn Area Emergency Response). (2020). Soil Burn Severity Dataset for the CAMERON PEAK Fire occurring on the Arapaho & Roosevelt National Forests/Pawnee National Grassland National Forest. USDA Forest Service.

Benavides-Solorio, J.D., MacDonald, L.H. (2001). Post-fire runoff and erosion from simulated rainfall on small plots, Colorado Front Range. Hydrological Processes 15, 2931–2952.

Benavides-Solorio, J.D., MacDonald, L.H. (2005). Measurement and prediction of post-fire erosion at the hillslope scale, Colorado Front Range. International Journal of Wildland Fire 14, 457–474.

Brasington, J., Langham, J., Rumsby, B. (2003). Methodological sensitivity of morphometric estimates of coarse fluvial sediment transport. Geomorphology 53 (3- 4), 299–316.

Breiman, L. (2001). Random Forests. Machine learning, 45, 5-32.

Brogan, D. J., MacDonald, L. H., Nelson, P. A., & Morgan, J. A. (2019). Geomorphic complexity and sensitivity in channels to fire and floods in mountain catchments. Geomorphology, 337, 53-68.

Cannon, S., Bigio, E., Mine, E., 2001. A process for fire-related debris flow initiation, Cerro Grande fire, New Mexico. Hydrol. Process. 15, 2011–3023.

Chapman, S.S., Griffith, G.E., Omernik, J.M., Price, A.B., Freeouf, J., and Schrupp, D.L. (2006). *Ecoregions of Colorado* (Map). Reston, Virginia, USGS.

Colorado Climate Center, Colorado State University, https://climate.colostate.edu

Congedo, Luca, (2021). Semi-Automatic Classification Plugin: A Python tool for the download and processing of remote sensing images in QGIS. Journal of Open Source Software, 6(64), 3172.

Cook, K. L. (2017). An evaluation of the effectiveness of low-cost UAVs and structure from motion for geomorphic change detection. Geomorphology 278, 195–208. doi:10.1016/j.geomorph.2016.11.009

Cook, K. L., and Dietze, M. (2019). Short Communication: a simple workflow for robust low-cost UAV-derived change detection without ground control points. *Earth Surf. Dyn.* 7, 1009–1017.

de Haas, T., Nijland, W., McArdell, B. W., & Kalthof, M. W. (2021). Case report: Optimization of topographic change detection with UAV structure-from-motion photogrammetry through survey co-alignment. Frontiers in Remote Sensing, 2, 5.

de Vente, J., Poesen, J. (2005). Predicting soil erosion and sediment yield at the basin scale: Scale issues and semi-quantitative models. Earth-Science Reviews 71 (1–2), 95–125.

Fernández, C., Vega, J.A., Jiménez, E., Fonturbel, T. (2011). Effectiveness of three post-fire treatments at reducing soil erosion in Galicia (NW Spain). International Journal of Wildland Fire 20, 104-114.

Foltz, R.B., Wagenbrenner, N.S. (2010). An evaluation of three wood shred blends for post-fire erosion control using indoor simulated rain events on small plots. Catena 80, 86–94.

Gartner, J. E., Cannon, S. H., & Santi, P. M. (2014). Empirical models for predicting volumes of sediment deposited by debris flows and sediment-laden floods in the Transverse Ranges of southern California. Engineering Geology, 176, 45–56.

Ghosal, K., Das Bhattacharya, S. (2020). A Review of RUSLE Model. J Indian Soc Remote Sens 48, 689–707 (2020).

Girona-García, A., Vieira, D. C., Silva, J., Fernández, C., Robichaud, P. R., & Keizer, J. J. (2021). Effectiveness of post-fire soil erosion mitigation treatments: A systematic review and meta-analysis. Earth-Science Reviews, 217, 103611.

Hubbert, K.R., Wohlgemuth, P.M., Beyers, J.L., 2012. Effects of hydromulch on post-fire erosion and plant recovery in chaparral shrublands of southern California. International Journal of Wildland Fire 21, 155–167.

Iowa Environmental Mesonet. Multi-RADAR Multi-Sensor (MRMS) Archiving. Iowa State University. https://mesonet.agron.iastate.edu/archive/

James, M. R., Antoniazza, G., Robson, S., and Lane, S. N. (2020). Mitigating systematic error in topographic models for geomorphic change detection: accuracy, precision and considerations beyond off-nadir imagery. Earth Surf. Process. Landforms, 45: 2251– 2271.

Johansen, M.P., Hakonson, T.E. and Breshears, D.D. (2001). Post-fire runoff and erosion from rainfall simulation: contrasting forests with shrublands and grasslands. Hydrol. Process., 15: 2953-2965.

Kim, C.-G., Shin, K., Joo, K.Y., Lee, K.S., Shin, S.S., Choung, Y. (2008). Effects of soil conservation measures in a partially vegetated area after forest fires. Sci. Total Environ. 399, 158–164.

Lane, S.N., Westaway, R.M., Murray Hicks, D. (2003). Estimation of erosion and deposition volumes in a large, gravel-bed, braided river using synoptic remote sensing. Earth Surf. Proc. Land. 28 (3), 249–271.

Legleiter, C. J., Lawrence, R. L., Fonstad, M. A., Marcus, W. A., & Aspinall, R. (2003). Fluvial response a decade after wildfire in the northern Yellowstone ecosystem: a spatially explicit analysis. Geomorphology, 54(3-4), 119-136.

Miller, M.E., MacDonald, L.H., Robichaud, P.R., Elliot, W.J., 2011. Predicting post-fire hillslope erosion in forest lands of the western United States. Int. J. Wildland Fire 20 (8), 982–999.

Montgomery, D. R. and Buffington, J. M. (1997). Channel-reach morphology in mountain drainage basins, Geol. Soc. Am. Bull., 109, 596–611.

Moody, J. A., & Kinner, D. A. (2006). Spatial structures of stream and hillslope drainage networks following gully erosion after wildfire. Earth Surface Processes and Landforms: The Journal of the British Geomorphological Research Group, 31(3), 319-337.

Moody, J. A., & Martin, D. A. (2001). Initial hydrologic and geomorphic response following a wildfire in the Colorado Front Range. Earth Surface Processes and Landforms: The Journal of the British Geomorphological Research Group, 26(10), 1049-1070.

Moody, J. A., Shakesby, R. A., Robichaud, P. R., Cannon, S. H., & Martin, D. A. (2013). Current research issues related to post-wildfire runoff and erosion processes. Earth-Science Reviews, 122, 10-37.

Nota, E. W., Nijland, W., & de Haas, T. (2022). Improving UAV-SfM time-series accuracy by co-alignment and contributions of ground control or RTK positioning. International Journal of Applied Earth Observation and Geoinformation, 109, 102772.

Nyman, P., Box, W. A. C., Stout, J. C., Sheridan, G. J., Keesstra, S. D., Lane, P. N. J., and Langhans, C. (2020) Debris-flow-dominated sediment transport through a channel network after wildfire. Earth Surf. Process. Landforms, 45: 1155– 1167.

Orr, H. K. (1970). Runoff and erosion control by seeded and native vegetation on a forest burn: Black Hills, South Dakota (Vol. 60). Rocky Mountain Forest and Range Experiment Station, Forest Service, US Department of Agriculture.

Over, J.R., Ritchie, A.C., Kranenburg, C.J., Brown, J.A., Buscombe, D., Noble, T., Sherwood, C.R., Warrick, J.A., and Wernette, P.A. (2021). Processing coastal imagery with Agisoft Metashape Professional Edition, version 1.6—Structure from motion workflow documentation: U.S. Geological Survey Open-File Report 2021–1039, 46 p.

Pelletier, J. D., & Orem, C. A. (2014). How do sediment yields from post-wildfire debris-laden flows depend on terrain slope, soil burn severity class, and drainage basin area? Insights from airborne-LiDAR change detection. Earth Surface Processes and Landforms, 39(13), 1822–1832.

Prats, S. A., González-Pelayo, Ó., Silva, F. C., Bokhorst, K. J., Baartman, J. E., & Keizer, J. J. (2019). Post-fire soil erosion mitigation at the scale of swales using forest logging residues at a reduced application rate. Earth Surface Processes and Landforms, 44(14), 2837-2848.

PRISM Climate Group, Oregon State University, http://prism.oregonstate.edu

Prosdocimi, M., Tarolli, P., & Cerdà, A. (2016). Mulching practices for reducing soil water erosion: A review. Earth-Science Reviews, 161, 191–203.

Rathburn, S. L., Shahverdian, S. M., & Ryan, S. E. (2018). Post-disturbance sediment recovery: Implications for catchment resilience. Geomorphology, 305, 61-75.

Renard, K. G., Foster, G. R., Weesies, G. A., & Porter, J. P. (1991). RUSLE: Revised universal soil loss equation. Journal of soil and Water Conservation, 46(1), 30-33.

Rengers, F. K., McGuire, L. A., Kean, J. W., Staley, D. M., Dobre, M., Robichaud, P. R., & Swetnam, T. (2021). Movement of sediment through a burned landscape: Sediment volume observations and model comparisons in the San Gabriel Mountains, California, USA. Journal of Geophysical Research: Earth Surface, 126, e2020JF006053.

Robichaud, P.R., Beyers, J.L., Neary, D.G. (2000). Evaluating the Effectiveness of Postfire Rehabilitation Treatments. General Technical Report, RMRS-GTR-63. U.S. Department of Agriculture, Forest Service, Rocky Mountain Research Station, Fort Collins, CO.

Robichaud P.R. (2005). Measurement of post-fire hillslope erosion to evaluate and model rehabilitation treatment effectiveness and recovery. International Journal of Wildland Fire 14, 475-485.

Robichaud, P.R., Ashmun, L.E., Sims, B.D. (2010a). Post-Fire Treatment Effectiveness for Hillslope Stabilization. General Technical Report, RMRS-GTR-240. U.S. Department of Agriculture, Forest Service, Rocky Mountain Research Station, Fort Collins, CO.

Robichaud, P. R., Lewis, S. A., Wagenbrenner, J. W., Ashmun, L. E., & Brown, R. E. (2013). Post-fire mulching for runoff and erosion mitigation: Part I: Effectiveness at reducing hillslope erosion rates. CATENA, 105, 75–92.

Robichaud, P. R., Wagenbrenner, J. W., Lewis, S. A., Ashmun, L. E., Brown, R. E., & Wohlgemuth, P. M. (2013). Post-fire mulching for runoff and erosion mitigation Part II: Effectiveness in reducing runoff and sediment yields from small catchments. Catena, 105, 93-111.

Rolstad, C., Haug, T., Denby, B. (2009). Spatially integrated geodetic glacier mass balance and its uncertainty based on geostatistical analysis: application to the western Svartisen ice cap, Norway. J. Glaciol. 55 (192), 666–680.

Schmeer, S. R., Kampf, S. K., MacDonald, L. H., Hewitt, J., & Wilson, C. (2018). Empirical models of annual post-fire erosion on mulched and unmulched hillslopes. Catena, 163, 276-287.

Shahverdian, S. (2015). Controls on Post-High Park Fire Channel Response, South Fork Cache la Poudre Basin, Colorado. M.S. thesis. Colorado State University.

Serifoglu Yilmaz, C., Yilmaz, V., & Güngör, O. (2018). Investigating the performances of commercial and non-commercial software for ground filtering of UAV-based point clouds. International Journal of Remote Sensing, 39(15-16), 5016-5042.

Soil Survey Staff: Natural Resources Conservation Service, United States Department of Agriculture. Web Soil Survey, available at: https://websoilsurvey.sc.egov.usda.gov/, last access: 1 July 2022.

Stoof, C. R., Vervoort, R. W., Iwema, J., Van Den Elsen, E., Ferreira, A. J. D., & Ritsema, C. J. (2012). Hydrological response of a small catchment burned by experimental fire. Hydrology and Earth System Sciences, 16(2), 267-285.

Štroner, M., Urban, R., Lidmila, M., Kolář, V., & Křemen, T. (2021). Vegetation filtering of a steep rugged terrain: The performance of standard algorithms and a newly proposed workflow on an example of a railway ledge. Remote Sensing, 13(15), 3050.

Wagenbrenner, J.W., MacDonald, L.H., Rough, D. (2006). Effectiveness of three post-fire rehabilitation treatments in the Colorado Front Range. Hydrological Processes 20, 2989–3006.

Wilson, C., Kampf, S. K., Wagenbrenner, J. W., & MacDonald, L. H. (2018). Rainfall thresholds for post-fire runoff and sediment delivery from plot to catchment scales. Forest ecology and management, 430, 346-356.

Wischmeier, W.H., Smith, D.D. (1978). Predicting Rainfall Erosion Losses – A Guide to Conservation Planning. U.S. Department of Agriculture (Handbook No. 537).

Workman, J. B., Cole, J. C., Shroba, R. R., Kellogg, K. S., & Premo, W. R. (2018). *Geologic map of the Fort Collins 30′×60′ quadrangle, Larimer and Jackson Counties, Colorado, and Albany and Laramie Counties, Wyoming*. USGS.

Zhang, J., Howard, K., Langston, C., Kaney, B., Qi, Y., Tang, L., Grams, H., Wang, Y., Cockcks, S., Martinaitis, S., Arthur, A., Cooper, K., Brogden, J., & Kitzmillller, D. (2016). Multi-Radar Multi-Sensor (MRMS) quantitative precipitation estimation: Initial operating capabilities. *Bulletin of the American Meteorological Society*, *97*(4), 621–638. https://doi.org/10.1175/BAMS-D-14-00174.1

Zipper, S. C., Hammond, J. C., Shanafield, M., Zimmer, M., Datry, T., Jones, C. N., ... & Allen, D. C. (2021). Pervasive changes in stream intermittency across the United States. Environmental Research Letters, 16(8), 084033.